Monthly Notices
of the
ROYAL ASTRONOMICAL SOCIETY
MNRAS **490,** 2219–2227 (2019) doi:10.1093/mnras/stz2630

Discovery of s-process enhanced stars in the LAMOST survey

Brodie J. Norfolk,[1]★ Andrew R. Casey,[2,3] Amanda I. Karakas,[2] Matthew T. Miles,[2] Alex J. Kemp,[2] Kevin C. Schlaufman,[4] Melissa Ness,[5] Anna Y. Q. Ho,[6] John C. Lattanzio[2] and Alexander P. Ji[7]†

[1]*Centre for Astrophysics and Supercomputing (CAS), Swinburne University of Technology, Hawthorn, Victoria 3122, Australia*
[2]*Monash Centre for Astrophysics (MoCA) and School of Physics and Astronomy, Monash University, Clayton Vic 3800, Australia*
[3]*Faculty of Information Technology, Monash University, Clayton 3800, Victoria, Australia*
[4]*Department of Physics and Astronomy, Johns Hopkins University, 3400 N Charles St, Baltimore, MD 21218, USA*
[5]*Department of Astronomy, Columbia University, 550 West 120th Street New York, NY 10027, USA*
[6]*Cahill Center for Astrophysics, California Institute of Technology, MC 249-17, 1200 E California Blvd, Pasadena, CA 91125, USA*
[7]*The Observatories of the Carnegie Institution for Science, 813 Santa Barbara St, Pasadena, CA 91101, USA*

Accepted 2019 September 13. Received 2019 September 13; in original form 2018 March 2

ABSTRACT

Here we present the discovery of 895 s-process-rich candidates from 454 180 giant stars observed by the Large Sky Area Multi-Object Fibre Spectroscopic Telescope (LAMOST) using a data-driven approach. This sample constitutes the largest number of s-process enhanced stars ever discovered. Our sample includes 187 s-process-rich candidates that are enhanced in both barium and strontium, 49 stars with significant barium enhancement only and 659 stars that show only a strontium enhancement. Most of the stars in our sample are in the range of effective temperature and log g typical of red giant branch (RGB) populations, which is consistent with our observational selection bias towards finding RGB stars. We estimate that only a small fraction ($\sim$0.5 per cent) of binary configurations are favourable for s-process enriched stars. The majority of our s-process-rich candidates (95 per cent) show strong carbon enhancements, whereas only five candidates ($<$3 per cent) show evidence of sodium enhancement. Our kinematic analysis reveals that 97 per cent of our sample are disc stars, with the other 3 per cent showing velocities consistent with the Galactic halo. The scaleheight of the disc is estimated to be $z_{\rm h} = 0.634 \pm 0.063$ kpc, comparable with values in the literature. A comparison with yields from asymptotic giant branch (AGB) models suggests that the main neutron source responsible for the Ba and Sr enhancements is the ^{13}C(α,n)^{16}O reaction. We conclude that s-process-rich candidates may have received their overabundances via mass transfer from a previous AGB companion with an initial mass in the range 1–3 M$_\odot$.

Key words: stars: abundances – stars: chemically peculiar.

1 INTRODUCTION

The abundance of elements created through the slow neutron capture process (s-process) is a measure of the nucleosynthetic reactions that occur primarily in asymptotic giant branch (AGB) stars. Because of their associated enrichment of the s-process element barium (Ba), stars with peculiar enhancements of carbon and heavy elements ($Z > 30$) are commonly referred to as 'barium stars' (Bidelman & Keenan 1951). The naming convention associated with barium stars is historical, and for the purposes of this paper it is necessary to clarify the definitions that will be used in subsequent discussions. Throughout the paper, we refer to stars with Ba and Sr enrichment as s-process-rich candidates, and stars with only strong Sr enrichment or only strong Ba enrichment as Sr-rich or Ba-rich candidates, respectively. Metal-poor stars ([Fe/H] < -1.2) enriched by s-process elements are typically referred to as CH stars in the literature; here, we simply describe our discoveries within this metallicity range as metal-poor s-process-rich candidates.

Extrinsic or intrinsic mechanisms can be invoked to explain s-process enrichment in a given star. This refers to the source of the enrichment: either a mechanism intrinsic to the star (e.g. an internal nuclear process) or an extrinsic process (e.g. pollution by stellar winds from a binary companion) that results in an overabundance of s-process elements. Both intrinsic and extrinsic mechanisms for enhancement may contribute somewhat to the known population of s-process enhanced stars.

★ E-mail: brodiejamesnorfolk@gmail.com
† Hubble Fellow.

Stars intrinsically enhanced in s-process elements are in the thermally pulsing AGB (TP-AGB) phase of stellar evolution. During this stage of evolution, nucleosynthesis occurring in the helium shell, followed by subsequent mixing, can result in an overabundance of carbon and s-process elements (Herwig 2005; Karakas & Lattanzio 2014) at the surface. Extrinsic enhancement occurs according to the mass-transfer hypothesis, which assumes that extrinsic s-process stars can be formed by stellar wind accretion (Boffin & Jorissen 1988; Jorissen & Boffin 1992; Han et al. 1995) or by Roche lobe overflow (Webbink 1986; Han et al. 1995) on to a lower-mass main-sequence companion. This hypothesis also assumes that the currently observed s-rich star is in a binary system and has received the overabundance of heavy elements from an AGB companion that has since evolved into a white dwarf. In fact, radial-velocity observations of s-rich stars show long-term velocity variations (McClure 1983), suggesting that all barium stars are in binary systems. For these reasons, the properties and occurrence rates of s-process enrichments in RGB populations are informative about the binary star fraction as a function of metallicity and the mass ratio of binary stars, as well as showing how AGB yields vary across a wide range of initial masses and metallicities.

The s-process synthesizes roughly half of all elements heavier than iron (e.g. Busso, Gallino & Wasserburg 1999; Travaglio et al. 2001; Herwig 2005; Bisterzo et al. 2014; Karakas & Lattanzio 2014). During the TP-AGB phase, thermal instabilities occur in the He shell every 10^5 yr or so, depending on the mass of the H-exhausted core. These bursts of energy drive a convective zone across almost the entire region lying between the base of the He-shell and H-shell. This mixes the products of nucleosynthesis within these regions while causing a radial expansion, pushing the H-shell out to cooler regions (Karakas, Lattanzio & Pols 2002). Following a thermal pulse, the convective envelope can then move inwards, towards regions previously mixed by the convective zones driven by the thermal pulse. This inward movement of the convective envelope is known as the third dredge-up (TDU), and can occur after each thermal pulse. During the TP-AGB phase, the TDU is responsible for the surface enrichment in ^{12}C and heavy elements produced by the s-process (e.g. Busso et al. 2001). Following the TDU, the star contracts, reigniting the H-shell and preventing further mixing to the surface. The interpulse, thermal pulse and dredge-up cycle can occur many times.

The progenitors of s-process-rich stars evolve from a metallicity-dependent initial mass range of approximately 0.8–8 $M_\odot$ (Karakas & Lugaro 2016). The minimum mass (0.8 $M_\odot$) of these progenitor AGB stars is defined by the onset of core helium burning while the maximum (8 $M_\odot$) is determined by the onset of core carbon burning. The age of these progenitor stars varies considerably, with lower-mass stars reaching ages $\approx$12 Gyr in metal-poor globular clusters. More massive metal-rich stars can have ages of less than $\approx$ 100 Myr, including progenitor stars that are at the core carbon burning limit or very close to it (e.g. Whitelock et al. 2013).

The majority of s-process-rich stars are observed to be members of the disc. Gomez et al. (1997) find that 90 per cent of their 318 barium stars have velocities characteristic of the disc, Pereira et al. (2011) find that their sample of 12 barium stars is fully consistent with disc membership and de Castro et al. (2016) find that 90 per cent of their 182 barium stars populate the Galactic disc. Jorissen et al. (1993) relate galactic position to the extrinsic or intrinsic nature of their s-process-rich stars. They show that intrinsic s-process-rich stars are concentrated towards the galactic plane, whereas extrinsic s-process-rich stars are uniformly distributed in absolute galactic latitude.

In this paper, we analyse 454 180 giant stars from the second data release of the Large Sky Area Multi-Object Fibre Spectroscopic Telescope (LAMOST) survey (Bai et al. 2016). We identify 895 s-process-rich candidates using a data-driven approach that involved filtering for significant flux residuals at the Sr and Ba lines. In Section 2, we describe our observations and the candidate selection process. In Section 3, we give details of our analysis of the high-resolution follow-up observations obtained for a few candidates. In Section 4, we discuss the properties of our s-process-rich candidates in the context of the existing body of literature. We provide concluding remarks in Section 5.

2 METHODS

2.1 LAMOST analysis

2.1.1 Data-driven analysis

The LAMOST survey released low-resolution ($\mathcal{R} \approx 1800$) optical spectra (3700–9000 Å) for 2 207 189 stars in their second data release (Bai et al. 2016). For details regarding the LAMOST atmospheric parameters and error analysis, we direct the reader to the LAMOST Stellar Parameter pipeline (Wu et al. 2011a,b; Bai et al. 2016). Stellar parameters and abundances ($T_{\rm eff}$, log g, [M/H], [α/M]) were derived by Ho et al. (2017) using The Cannon (Ness et al. 2015, 2016; Casey et al. 2016). This involved label transfer (a process for improving the accuracy of parameters and abundances in one survey using the results from another) from APOGEE to LAMOST. This was accomplished using 9952 giant stars in common as a training sample to generate a predictive model, which was then applied to the stars that make up our sample of 454 180 stars. As a consequence of this procedure, our sample is limited to giant stars, and we are therefore unable to identify s-process enhanced dwarf stars. Cross-validation tests between low-resolution ($\mathcal{R} \approx 1800$) LAMOST spectra and higher-resolution ($\mathcal{R} \approx 22\,500$) APOGEE spectra substantially reduce the inconsistencies and label uncertainties between each individual survey. The typical uncertainties are approximately 70 K in effective temperature $T_{\rm eff}$, 0.1 dex in surface gravity log g, 0.1 dex in metallicity [M/H] and 0.04 dex in the abundance of α-elements relative to overall metallicity [α/M]. These uncertainties are comparable with those present in APOGEE (Alam et al. 2015).

2.1.2 Candidate selection

The s-process-rich candidates in this work were identified by filtering for significant flux residuals at the Sr and Ba lines. We categorize each spectrum as s-process enriched, Ba-enriched or Sr-enriched. We fit a Gaussian function with amplitude A to the residuals of the observed flux and the data-driven model from The Cannon, and the standard deviation σ_A at wavelengths 4554 Å (Ba II) and 4077 Å (Sr II) for s-process-rich candidates, at wavelengths 4554 Å (Ba II) and 4934 Å (Ba II) for Ba-enriched candidates, and at wavelengths 4077 Å (Sr II) and 4215 Å (Sr II) for Sr-enriched candidates. The amplitude of each Gaussian fit at each wavelength is a measure of the depth of each absorption line relative to what is expected of a star of that metallicity, alpha-abundance, effective temperature and log g. If the observed spectrum has deeper absorption lines than the model at the corresponding wavelengths, it

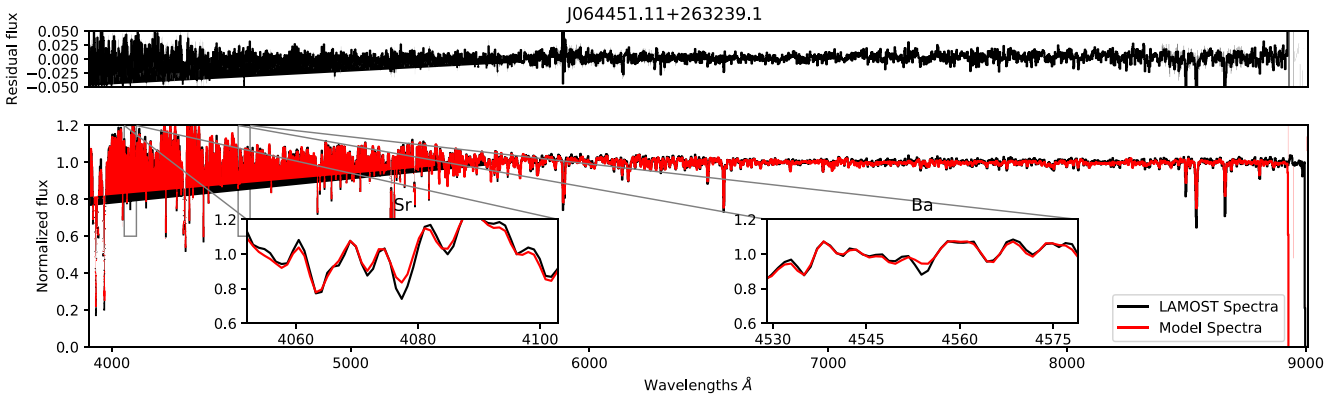

Figure 1. Pseudo-continuum-normalized LAMOST spectra for the s-process candidate J064451.11+263239.2. The data are shown in black and the best-fitting data-driven model is shown in red. We include zoom-in axes to show significant deviations in Sr and Ba at 4077 and 4554 Å, respectively.

Table 1. Properties of the 895 s-process-rich candidates. The table is available online in its entirety, but here we show a portion to demonstrate its style and content.

2MASS ID	RA (J2000)	Dec. (J2000)	v_r (km s^{-1})	S/N (pixel^{-1})	$T_{\rm eff}$ (K)	log g	[Fe/H]	[α/Fe]	χ_r^2	[Ba/Fe]	[Sr/Fe]	Ba II	Sr II	Ba II and Sr II
J000019.26+501444.8	00:00:19.27	+ 50:14:44.9	− 3.9	49	4973	3.27	0.21	0.08	0.66	0.25	0.83	✗	✓	✗
J000020.55+411348.1	00:00:20.56	+ 41:13:48.2	− 28.2	32	4882	2.74	− 0.22	0.04	0.23	− 0.17	0.90	✗	✓	✗
J000134.95+490743.2	00:01:34.96	+ 49:07:43.2	− 42.3	72	5044	3.11	− 0.54	0.11	0.79	1.02	0.45	✗	✗	✓
J000258.09+410730.0	00:02:58.10	+41:07:30.1	− 34.5	41	4697	2.57	− 0.22	0.12	0.98	− 0.10	0.80	✗	✓	✗
J000403.80+160257.1	00:04:03.80	+16:02:57.2	− 35.4	42	5200	3.40	− 0.41	0.09	0.33	0.92	0.52	✗	✗	✓
J000439.16+183350.3	00:04:39.17	+18:33:50.4	− 38.7	31	4601	2.50	0.44	0.03	0.34	− 0.11	0.88	✗	✓	✗
J000444.87+400402.1	00:04:44.88	+40:04:02.1	− 94.7	53	4172	1.46	− 0.08	0.09	0.72	0.03	0.91	✗	✓	✗
J000552.76+261849.3	00:05:52.76	+26:18:49.4	− 22.5	73	4924	3.14	− 0.05	0.09	0.67	0.28	0.85	✗	✓	✗
J000737.70+394055.5	00:07:37.70	+39:40:55.6	− 31.5	33	4700	2.80	− 0.04	0.07	0.28	− 0.13	0.81	✗	✓	✗

is considered a candidate with an enhancement. A randomly chosen s-process candidate is shown in Fig. 1.

We used five criteria for each spectrum and subsequent set of absorption lines in order to identify potential s-process enrichment.

(i) The profile amplitude A for both enhanced lines must be $\Delta A < -0.05$, indicating a stronger absorption line than expected by the model.

(ii) Both amplitudes must be measured within three standard deviations of the profile amplitude ($|\Delta A|/\sigma_A > 3$).

(iii) The wavelength at each (Doppler-corrected) absorption line must be within 2 Å ($\Delta\lambda < 2$ Å) of the rest-frame laboratory wavelength.

(iv) The reduced χ^2 from The Cannon must satisfy $\chi_r^2 < 3$.

(v) The LAMOST spectra must have a signal-to-noise ratio (S/N) of >30 pixel^{-1}.

In addition to requiring matches at two wavelengths (e.g. both 4934 and 4554 Å for Ba-enriched candidates), we visually inspected all candidates to exclude spectra with data reduction issues, apparent absorption finer than the spectral resolution, or overly noisy spectra. This approach yielded 895 candidates, the details of which are listed in Table 1, including 187 s-process-rich candidates, 49 Ba-enriched stars and 659 stars with just Sr enrichment. This constitutes the largest collection of s-process enhanced stars ever discovered. The previous most numerous sample consists of 182 Ba-enriched (Ba II) stars presented by MacConnell, Frye & Upgren (1972).

For the remainder of this paper, we restrict our analysis to the 187 s-process-rich candidates that show enhancement in both Ba and Sr. While the 49 or 659 stars with only Ba or Sr enhancements (respectively) can also be classified as s-process-rich candidates, there might be other explanations for their chemical abundance pattern (e.g. Maiorca et al. 2011).

2.1.3 *Enhancements as a result of sodium, technetium and carbon*

Enhancements in sodium (Na), technetium (Tc) and carbon are useful for determining whether a sample is populated by AGB stars or by polluted extrinsic s-process-rich stars. We performed an identical analysis to the process described in Section 2.1.2 in order to identify negative flux residuals for enhancement in Na, Tc and carbon. For Na enrichment, we required significant absorption in the doublet lines at 5889 and 5895 Å. Only five out of 187 s-process-rich candidates met these criteria. For Tc enhancement, we searched for significant residual deviations at 4049, 4238, 4262, 4297 and 5924 Å. These absorption lines are extremely weak and a substantial amount of Tc enhancement would be required before it would become visible, even in a high S/N LAMOST spectrum. We found that 51 s-process-rich candidates exhibited some level of significant enhancement at the single absorption line 4238 Å. However, we caution that Tc enhancement is usually a very weak signature in such warm stars and would require multiple lines of enhancement; it is considerably blended by other s-process element lines (e.g. Van Eck & Jorissen 1999). As such, we discard these 51 stars with enhancement at a single Tc absorption line as false positives. For carbon enhancement, we searched for significant deviations at the G band of CH near 4300 Å, of which 178 out of 187 s-process-rich candidates exhibit significant flux residuals and are therefore considered carbon-enriched.

2.1.4 Abundances estimated from LAMOST spectra

We estimated [Ba/Fe] and [Sr/Fe] abundance ratios for all s-process-rich candidates by spectrum synthesis. We assumed that absorption due to most metal lines is captured by The Cannon model, and deviations in flux at the 4554 Å Ba II line and the 4077 Å Sr II transition are solely due to enhancements in Ba and Sr, respectively. We used the grid of MARCS model atmospheres (Gustafsson et al. 2008), atomic transitions from the Vienna Atomic Line Database (VALD; Kupka et al. 1999), and the SME code (Valenti & Piskunov 1996; Blanco-Cuaresma et al. 2014) to synthesize the spectra of each star. Then we varied the Ba and Sr abundances until they matched the flux deviations away from our data-driven model. We adopted the stellar parameters ($T_{\rm eff}$, $\log g$, [Fe/H]) from Ho et al. (2017), and assumed a microturbulence velocity of $v_{\rm mic} = 2\,{\rm km\,s^{-1}}$. Uncertainties in [Ba/Fe] and [Sr/Fe] from these spectra are taken as the fitting error due to noise, added in quadrature with an adopted 0.2 dex systematic error floor. We assume the same isotopic fractions from Sneden, Cowan & Gallino (2008). Previous studies have used a threshold of [Ba/Fe] $> +0.3$ to define an s-process-rich star (Malaney & Lambert 1988). Our abundance analysis shows that 186 out of 187 of our s-process-rich candidates – identified from flux residuals alone – meet this criterion based on spectrum synthesis of the 4554-Å transition. Table 1 lists a portion of our 895 s-process enhanced sample.

2.2 Dynamics

We integrated the galactic orbits using astrometry from the second data release (DR2) of *Gaia* (Prusti et al. 2016; Brown et al. 2018; Cropper et al. 2018; Katz et al. 2018; Lindegren et al. 2018; Sartoretti et al. 2018) for 871 out of 895 of the s-process enhanced stars with positive parallaxes ($\varpi > 0$) and parallax S/N of five or above ($\varpi/\sigma_{\varpi} > 5$). We integrated each star backwards for 0.5 Gyr using the GALA Python package (Price-Whelan 2017) in a Milky Way-like potential (Price-Whelan et al. 2014) that consists of three components: a Hernquist bulge and nucleus, a Miyamoto–Nagai disc and a Navarro–Frenk–White halo (Hernquist 1990; Miyamoto & Nagai 1975; Navarro, Frenk & White 1997). We computed spatial velocities relative to the local standard of rest, where $U_{\rm LSR}$ is positive towards the Galactic Centre, $V_{\rm LSR}$ is positive in the direction of Galactic rotation ($l = 90°$, $b = 0°$) and $W_{\rm LSR}$ is positive towards the North Galactic Pole ($b = 90°$). Our analysis revealed disc star membership of 97 per cent and halo star membership of 3 per cent.

3 FOLLOW-UP OBSERVATIONS WITH MAGELLAN/MIKE

3.1 Observations and data reduction

High-resolution spectra were obtained for two of the s-process-rich candidates (J09162834+0259348 and J08351472–0548480) using the Magellan Inamori Kyocera Echelle (MIKE; Bernstein et al. 2003) spectrograph on the Magellan Clay telescope (Schectman & Johns 2003) at Las Campanas Observatory, Chile. These two candidates were selected as targets of opportunity only, and do not represent a comprehensive follow-up observational campaign. We observed both stars in good seeing using the 0.7-arcsec slit and 2×2 spatial on-chip binning, providing a spectral resolution of $\mathcal{R} \approx 28\,000$. Exposure times of 100 s were sufficient to achieve a S/N ratio exceeding 30 pixel^{-1} at 4500 Å. We acquired calibration (biases, milky, quartz and Th–Ar arc lamp) frames in the afternoon. We reduced the data using the CARPY package (Kelson et al. 2000). We used spline functions to continuum-normalize all echelle orders, and we resampled the normalized spectra on to a uniform-spaced wavelength map. We used a rest-frame normalized template appropriate for an FGK-type star to place the observed spectra at rest.

3.2 Abundance analysis

We adopted the stellar parameters ($T_{\rm eff}$, $\log_{10} g$, [Fe/H]) provided from the data-driven analysis of Ho et al. (2017). Following the procedure outlined in Casey (2014), we measured the strength of Ba II (4554, 4934 and 6496 Å) and Sr II (4077 and 4215 Å) absorption lines by spectral synthesis, using s-process isotopic ratios from Sneden et al. (2008). The abundance ratios we estimate from high-resolution spectra are in excellent agreement with our estimates from LAMOST spectra, all agreeing within the joint 1.2σ.

For J09162834+0259348, from high- and low-resolution spectra, respectively, we find [Sr/Fe] $= 0.76 \pm 0.10$ and 0.85 ± 0.21, and [Ba/Fe] $= 0.92 \pm 0.10$ and 0.77 ± 0.21. The largest discrepancy we find between high- and low-resolution spectra is [Sr/Fe] for J08351472–0548480, where we find [Sr/Fe] $= 0.62 \pm 0.07$ from our Magellan/MIKE spectra, compared with 0.90 ± 0.22 from LAMOST. For J08351472–0548480, we also find [Ba/Fe] $= 0.94 \pm 0.12$ from high-resolution spectra and [Ba/Fe] $= 0.80 \pm 0.26$ from low-resolution spectra.

Uncertainties on abundances derived from high-resolution spectra are taken as the standard deviation of multiple line measurements. The high-resolution abundances that we find help to validate our methodology for candidate selection, and for estimating abundances from LAMOST spectra.

4 DISCUSSION

4.1 Extrinsic or intrinsic

The s-process enrichment can be explained by intrinsic or extrinsic mechanisms. Intrinsically enhanced s-process-rich stars must be massive enough to reach the TP-AGB phase within the age of the Galaxy, and extrinsic s-process stars should be members of a binary system where the companion is now a white dwarf. Evidence of a recent (< 1 Myr) mass pollution event can present itself as enrichment in both s-process elements and 99Tc. Fig. 2 shows that the majority of stars in our sample are within the temperature and surface gravity ranges consistent with the first giant branch. This figure highlights that our sample does not appear to contain many stars that have evolved enough to reach the TP-AGB phase so it must be composed primarily of extrinsic s-process-rich candidates. Candidates with $\log g \lesssim 2$ in Fig. 2 could be either AGB stars or RGB stars.

4.2 Frequency of s-process stars

We find that the frequency of s-process-rich stars among a well-defined sample of giants is ∼0.2 per cent, which is substantially lower than the canonical value of 1 per cent from MacConnell et al. (1972). The majority of our sample appears to consist of extrinsic s-process-rich candidates polluted by a presumed binary companion. Badenes et al. (2018) found that the multiplicity inferred from APOGEE observational data is best explained by assuming a binary fraction of ∼35 per cent, and Tian et al. (2018) estimate

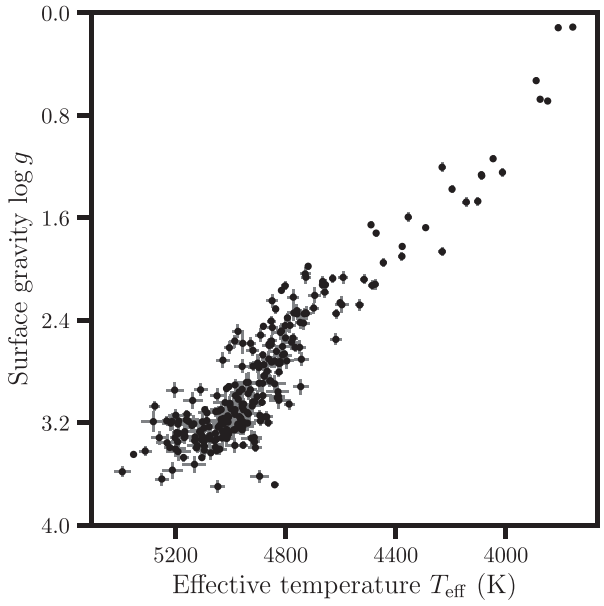

Figure 2. Effective temperature $T_{\rm eff}$ and surface gravity $\log g$ for 187 s-process-rich candidates from LAMOST.

a binary fraction of ∼50 per cent for solar-type stars in LAMOST data release 4. A fraction of those binary systems will become s-process enriched. However, we find that only 0.2 per cent of systems in our sample are s-process-rich. Therefore, taking the mean binary fraction estimate of 42.5 per cent, only ∼0.5 per cent of binary systems will end up as s-process enriched systems. This highlights that there is a set of constraining conditions that must be met in a binary system in order for it to result in an s-process-rich star (Jorissen et al. 2019). Binary stellar evolution theory should be able to provide information on these constraints, but the population synthesis and physical modelling required to produce such information is beyond the scope of this work.

4.3 Sodium enhancement

Sodium is produced by the Ne–Na cycle in any hydrogen-burning environment where the temperature exceeds about 30×10^6 K (Arnould, Goriely & Jorissen 2004). This includes the convective cores of intermediate-mass stars and the H-burning shells of AGB stars (El Eid & Champagne 1995; Mowlavi 1999; Karakas & Lattanzio 2003). The surface of the giant becomes enriched in Na via the first dredge-up, although predicted enrichments are small (of the order of 0.15 dex for $M \lesssim 4\,{\rm M}_\odot$), after second dredge-up where predicted enrichments are larger (Karakas & Lattanzio 2014), and during the AGB.

Intermediate-mass AGB stars that experience hot bottom burning are predicted to produce Na, but model predictions depend on uncertain physics (e.g. Ventura et al. 2013; Slemer et al. 2017). It is unclear if mass transfer from intermediate-mass AGB stars can produce an s-process candidate but it would likely be poor in carbon and fluorine, because of hot bottom burning, and rich in Sr over Ba (e.g. Karakas & Lugaro 2016). See Section 4.4 for further discussion.

Antipova et al. (2004) reported enhanced Na in three of their 16 RGB s-process-rich stars. They relate this to the first dredge-up of nuclear-burning material produced by convection during the RGB phase, and they suggest that [Na/Fe] ratios are systematically higher

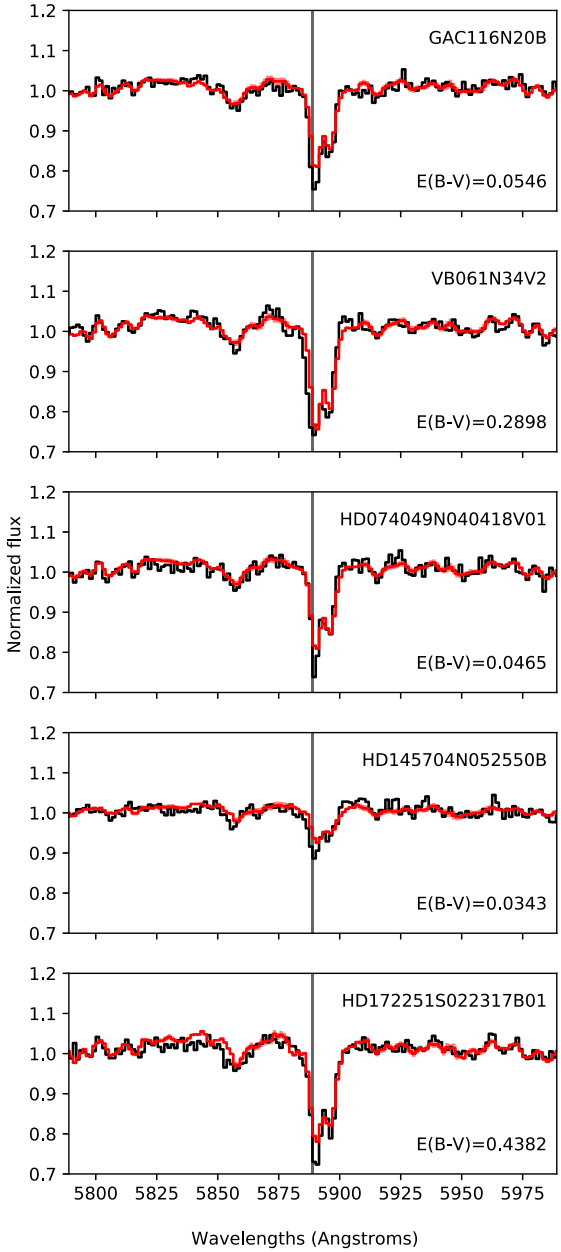

Figure 3. Pseudo-continuum-normalized LAMOST spectra for the s-process candidates enhanced in Na, as shown by the deviations in the doublet lines at 5889 and 5895 Å. The data are shown in black and the best-fitting data-driven model is shown in red.

for giants with lower $\log g$ values. Similarly, de Castro et al. (2016) propose a possible weak anticorrelation between the [Na/Fe] ratio and $\log g$, and they highlight that this trend is present in previous studies (e.g. Boyarchuk et al. 2002; Mishenina et al. 2006; Luck & Heiter 2007; Takeda, Sato & Murata 2008).

We find that only five out of 187 s-process-rich candidates (<3 per cent) exhibit enhanced Na, as shown in Fig. 3, and all five have $\log g \approx 3$. Moreover, it is likely that some of these stars appear to have high Na because the interstellar gas lines of Na are misinterpreted as stellar absorption. Using the *IRAS* all-sky dust map (Schlafly & Finkbeiner 2011), we find that two out of these five candidates have $E(B-V) \approx 0.35$, suggesting that the flux residuals around the Na doublet are a result of interstellar absorption.

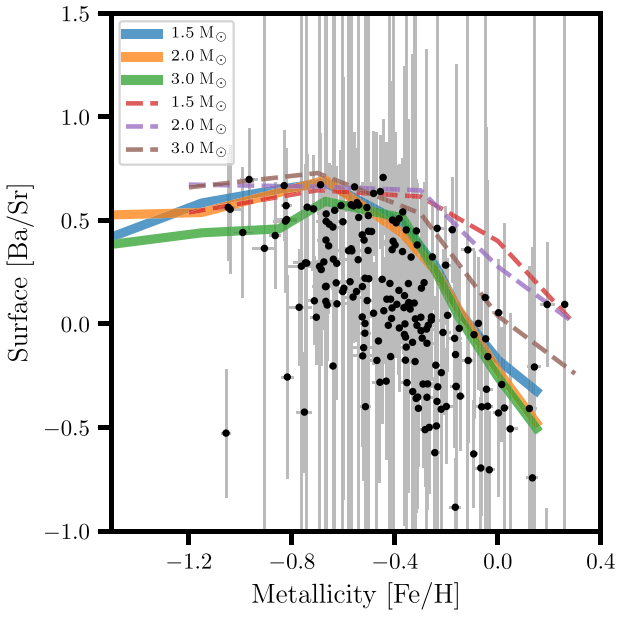

Figure 4. Metallicities ([Fe/H]; *x*-axis) and heavy-to-light s-process (hs/ls) abundance ratios ([Ba/Sr] as measured from LAMOST; *y*-axis) for 187 s-process-rich candidates. Blue, orange and green lines indicate surface [hs/ls] yields from Cristallo et al. (2015) for different masses. Red, purple and brown lines indicate surface [hs/ls] yields from Karakas & Lugaro (2016) for [Fe/H] at +0.3. 0.0 and –0.3; from Karakas et al. (2018) for [Fe/H] = −0.7; and from Fishlock et al. (2014) for [Fe/H] = −1.2.

However, three of these five candidates exhibit low (≈0.045) $E(B-V)$ values, indicating that enhancement is more likely a result of stellar absorption. These results suggest that Na-rich material from a companion TP-AGB star has polluted these three s-process-rich candidates. It also demonstrates that Na enhancement is by no means ubiquitous in s-process-rich candidates. We do not observe a correlation between [Na/Fe] and log *g* in our sample. We also find that s-process-rich candidates do not have higher [Na/Fe] abundance ratios, on average.

4.4 Comparison to AGB yields

Fig. 4 shows the [Ba/Sr] abundance ratio (for all 187 s-process candidates identified in LAMOST). Although the [Ba/Sr] ratio is quite noisy (∼0.6 dex mean value of the uncertainty), the overall metallicity [Fe/H] is quite precise (0.1 dex or better). The observed ratios of [Ba/Sr] shown in Fig. 4 are particularly interesting for comparison with theoretical predictions of the s-process because we are comparing two elements that are only produced in AGB stars. Lugaro et al. (2012) have discussed how the ratios of light to heavy s-process elements are essentially independent of stellar modelling uncertainties including TDU mixing, mass loss, and the accretion and mixing processes on the binary companion. Ratios between elements produced by neutron capture are a measure of the thermodynamic conditions occurring in the previous AGB star, the neutron source and the neutron flux.

In Fig. 4, we also show theoretical s-process predictions from two groups: the FRUITY[1] yields from Cristallo et al. (2015), which cover a range in metallicity from [Fe/H] ≈ 0.1 to −2.3, and the Monash yields (Fishlock et al. 2014; Karakas & Lugaro 2016), which cover a range in metallicity from [Fe/H] = +0.3 to −1.2 (similarly to Cseh et al. 2018). For both sets of models, we show results from initial masses between 1.5 and 3 $M_\odot$. Observational evidence suggests that the dominant polluters of s-process-rich candidates are low-mass AGB stars with masses below $\lesssim 4\,M_\odot$ where the main neutron source is the $C^{13}(\alpha,n)O^{16}$ reaction (e.g. Lugaro et al. 2012; Karinkuzhi et al. 2018).

Reasons for this include the fact that intermediate-mass stars over approximately 4 $M_\odot$ do not become carbon-rich on the AGB (or if they do, only at the very end), and the fact that intermediate-mass stars near solar metallicity are not predicted to produce much Ba at all. This is partly a consequence of the neutron source operating inside intermediate-mass stars; that is, the $Ne^{22}(\alpha,n)Mg^{25}$ source that favours production of Sr over Ba (e.g. Karakas & Lugaro 2016). It is unclear if the $C^{13}(\alpha,n)O^{16}$ neutron source, which dominates in low-mass AGB stars, also operates in intermediate-mass AGB stars; see discussions in Straniero, Cristallo & Piersanti (2014) and García-Hernández et al. (2013).

Stellar yields are the integrated mass expelled into the interstellar medium, and these represent an upper limit that includes surface abundance changes from all previous mixing events. Therefore, it is not surprising that the yield predictions are in the upper range of the observed ratios. Mass transfer from an AGB star to a companion does not necessarily occur right at the end of the AGB star's life. Mass transfer via a stellar wind can occur any time that the AGB star is losing mass via a sufficiently strong wind, and mass transfer via Roche lobe overflow can occur at any time during the AGB phase, regardless of whether the star is experiencing significant wind mass loss; see population synthesis studies of peculiar stars (e.g. Han et al. 1995; Karakas, Tout & Lattanzio 2000; Abate et al. 2013, 2015; Liu et al. 2018).

For example, if we examine the 2-$M_\odot$, [Fe/H] = 0 model from Karakas & Lugaro (2016) and calculate the [Ba/Sr] ratio as a function of TDU mixing episodes, we see that the ratio increases from 0.05 at the first mixing event to 0.24 by the second, before reaching a constant value of 0.35 by the sixth. Ratios of [Ba/Sr] < 0 are not predicted from low-mass AGB models that become carbon-rich, which is a consequence of the $C^{13}(\alpha,n)O^{16}$ neutron source causing high neutron exposures and element production at the Ba and Pb peaks (e.g. Busso et al. 2001). It is possible for an intermediate-mass AGB star to produce [Ba/Sr] < 0, for example, the 5-$M_\odot$, [Fe/H] = −0.7 model from Karakas & Lugaro (2016) where the final [Ba/Sr] ≈ −0.4, in which case the overall [Ba/Fe] ≈ 0.1. Mass transfer from such an AGB companion would not produce a star that would be flagged as an s-process-rich candidate.

4.5 Dynamics

The majority of stars in our sample show prograde orbits that are consistent with membership in the Milky Way disc. Figs 5 and 6 illustrate the galactic velocities for all s-process-rich candidates in this work. For our entire sample, Fig. 5 shows that 97 per cent have velocities that are consistent with the disc, and just 3 per cent have velocities that are more consistent with the halo. Our sample has a similar dynamical make-up to previously published samples in the literature. Gomez et al. (1997) and de Castro et al. (2016) both present samples with thin disc membership of ∼90 per cent, and the sample of Pereira et al. (2011) with 12 s-process stars is fully consistent with disc membership. Jorissen et al. (1993) attribute the galactic position of s-process enhanced stars as dependent on their intrinsic or extrinsic nature (see their section 4.2). They estimate

[1] http://fruity.oa-teramo.inaf.it/

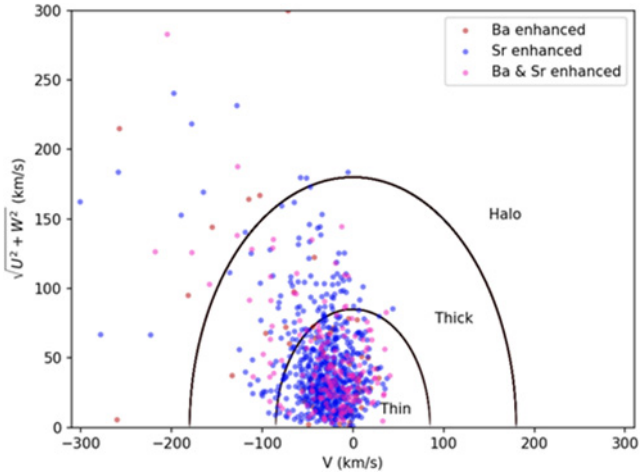

Figure 5. Galactic distribution represented by a Toomre diagram, spatial velocities (V in km s^{-1}; x-axis) and ($\sqrt{U^2+W^2}$ in km s^{-1}; y-axis) for a number of s-process-rich candidates with *Gaia* DR2 parallaxes. Red, blue and purple dots highlight Ba, Sr, and both Ba and Sr enhancement, respectively.

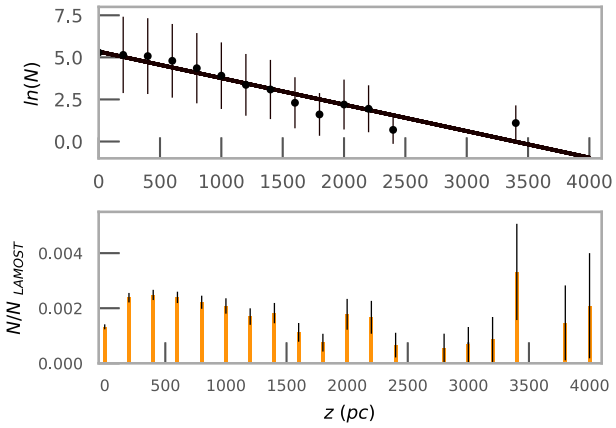

Figure 6. Top panel: the density distribution ln(N) (y-axis) as a function of z, $|z|$ (x-axis). Bottom panel: absolute z distribution, $|z|$ (x-axis) and the number of corresponding stars $N/N_{\rm LAMOST}$ (normalized per galactic bin; y-axis). Shown for the *Gaia* DR2 parallaxes of the s-process-rich candidates, and for the s-process-rich candidates as a fraction of the LAMOST sample with *Gaia* DR2 parallaxes.

the scaleheight for their intrinsic stars, and find that they are concentrated towards the galactic plane whilst their extrinsic s-process stars are uniformly distributed in absolute galactic latitude. Fig. 6 (top panel) shows the logarithmic distribution of the s-process-rich stars cross-matched with *Gaia* DR2 as a function of $|z|$. Here we derive the number density in bins of ∼0.2 kpc and the error bars shown for the y-axis are Poisson errors. Following an exponential-decay profile, we estimate a scaleheight of $z_{\rm h} = 0.634 \pm 0.063$ kpc, which is represented by the straight line in the figure. This is comparable with the $z_{\rm h} = 0.637^{0.056}_{-0.036}$ kpc result estimated by Wang et al. (2018) for thick disc stars at $R = 8$ kpc in the LAMOST DR3 sample. However, our 97 per cent disc star sample is primarily comprised of thin disc stars, as seen in Fig. 5. If we remove the thick disc stars and recalculate the scaleheight, then the scaleheight for only the thin disc stars is estimated to be $z_{\rm h} = 0.498 \pm 0.049$ kpc. This is more consistent with previous scaleheight measurements for thin disc stars (i.e. 220–450 pc from Bland-Hawthorn & Gerhard 2016), and it demonstrates that the thick disc stars in our sample skew the entire sample's scaleheight measurement substantially. Fig. 6 (bottom panel) shows all absolute galactic z-positions for our sample. After developing a normalized histogram (per galactic bin) and correcting for the LAMOST selection function, we show the absolute galactic z-position when ignoring outlier bins where the s-process-rich candidates, as a fraction of the LAMOST sample, approach unity.

5 CONCLUSIONS

We have conducted the largest ever search for s-process enhanced stars using the LAMOST second data release. From 454 180 giant stars, we identify 895 s-process enhanced stars, including 187 s-process-rich candidates, 49 Ba-enriched stars and 659 stars with Sr enrichment. This sample size is the greatest number of s-process-rich candidates known. We estimate only a small fraction (∼0.5 per cent) of binary configurations are favourable for s-process enriched stars. We found that 97 per cent of our sample have velocities that are consistent with disc membership, and just 3 per cent have velocities more consistent with the halo. The scaleheight for our entire sample is calculated to be $z_h = 0.634 \pm 0.063$ kpc.

We find the majority (95 per cent) of our s-process candidates show carbon enhancement. Contrary to previous studies, we do not find s-process-rich candidates to have significantly higher [Na/Fe] than Milky Way field giants. Only five (<3 per cent) of our s-process-rich candidates show enhancement in Na, and the flux residuals in two of those are likely to be a result of interstellar gas. We suggest that systematic effects in measuring [Na/Fe] from stars with low log g in previous works contributed to the discrepancy with our results, as well as comparisons between studies that make use of different abundance analysis techniques.

Despite our noisy estimates of [Ba/Fe] and [Sr/Fe] from LAMOST spectra, comparisons with AGB yields indicate the main neutron source responsible for s-process enhancement is consistent with the $C^{13}(\alpha,n)O^{16}$ reaction chain. Theoretical yields suggest the progenitors of our s-process enhanced sample are low-mass AGB stars between 1 and 3 $M_\odot$. We encourage follow-up high-resolution spectrographic observations to measure a full suite of neutron-capture abundances precisely and to perform a comprehensive comparison of AGB star models.

ACKNOWLEDGEMENTS

This paper includes data gathered with the 6.5-m Magellan Telescope located at Las Campanas Observatory, Chile. We thank David W. Hogg (NYU) and Hans-Walter Rix (MPIA) for useful discussions. ARC is supported through an Australian Research Council Discovery Project under grant DP160100637. AIK acknowledges financial support from the Australian Research Council (DP170100521). AYQH was supported by the GROWTH project funded by the National Science Foundation under PIRE Grant No 1545949, and a National Science Foundation Graduate Research Fellowship under Grant No. DGE-1144469. APJ is supported by NASA through Hubble Fellowship grant HST-HF2-51393.001 awarded by the Space Telescope Science Institute, which is operated by the Association of Universities for Research in Astronomy, Inc., for NASA, under contract NAS5-26555. This research has made use of NASA's Astrophysics Data System. The Guoshoujing

Telescope (LAMOST) is a National Major Scientific Project built by the Chinese Academy of Sciences. Funding for the project has been provided by the National Development and Reform Commission. LAMOST is operated and managed by the National Astronomical Observatories, Chinese Academy of Sciences. This work has made use of data from the European Space Agency (ESA) mission *Gaia* (https://www.cosmos.esa.int/gaia), processed by the *Gaia* Data Processing and Analysis Consortium (DPAC, https://www.cosmos.esa.int/web/gaia/dpac/consortium). Funding for the DPAC has been provided by national institutions, in particular the institutions participating in the *Gaia* Multilateral Agreement.

REFERENCES

Abate C., Pols O. R., Izzard R. G., Mohamed S. S., de Mink S. E., 2013, A&A, 552, A26
Abate C., Pols O. R., Stancliffe R. J., Izzard R. G., Karakas A. I., Beers T. C., Lee Y. S., 2015, A&A, 581, A62
Alam S. et al., 2015, ApJS, 219, 12
Antipova L. I., Boyarchuk A. A., Pakhomov Yu. V., Panchuk V. E., 2004, Astron. Rep., 48, 597
Arnould M., Goriely S., Jorissen A., 1999, A&A, 347, 572
Badenes C. et al., 2018, ApJ, 854, 147
Bai Z. R. et al., 2016, Res. Astron. Astrophys., 16, 107
Bernstein R., Shectman S. A., Gunnels S. M., Mochnacki S., Athey A. E., 2003, Proc. SPIE, 4841, 1694
Bidelman W. P., Keenan P. C., 1951, ApJ, 114, 473
Bisterzo S., Travaglio C., Gallino R., Wiescher M., Käppeler F., 2014, ApJ, 787, 10
Blanco-Cuaresma S., Soubiran C., Heiter U., Jofré P., 2014, A&A, 569, A111
Bland-Hawthorn J., Gerhard G., 2016, ARA&A, 54, 529
Boffin H. M. J., Jorissen A., 1988, A&A, 205, 155
Boyarchuk A. A., Pakhomov Y. V., Antipova L. I., Boyarchuk M. E., 2002, Astron. Rep., 46, 819
Brown A. G. A.(Gaia Collaboration) et al., 2018, A&A, 616, 1
Busso M., Gallino R., Lambert D. L., Travaglio C., Smith V. V., 2001, ApJ, 557, 802
Busso M., Gallino R., Wasserburg P. C., 1999, ARA&A, 37, 239
Casey A. R., 2014, PhD thesis, Australian National University
Casey A. R., Hogg D. W., Ness M., Rix H.W., Ho A. Q. Y., Gilmore G., 2016, preprint (arXiv:1603.03040)
Cristallo S., Straniero O., Piersanti L., Gobrecht D., 2015, ApJ, 219, 40
Cropper M. et al., 2018, A&A, 616, A5
Cseh B. et al., 2018, A&A, 620, A146
de Castro D. B., Pereira C. B., Roig F., Jilinski E., Drake N. A., Chavero C., Sales Silva J. V., 2016, MNRAS, 459, 4299
El Eid M. F., Champagne A. E., 1995, ApJ, 451, 298
Fishlock C. K., Karakas A. I., Lugaro M., Yong D., 2014, ApJ, 797, 44
García-Hernández D. A., Zamora O., Yagüe A., Uttenthaler S., Karakas A. I., Lugaro M., Ventura P., Lambert D. L., 2013, A&A, 555, L3
Gomez A. E., Luri X., Grenier S., Prevot L., Mennessier M. O., Figueras F., Torra J., 1997, A&A, 319, 881
Gustafsson B., Edvardsson B., Eriksson K., Jørgensen U. G., Nordlund Å., Plez B., 2008, A&A, 486, 951
Han Z., Eggleton P. P., Podsiadlowski P., Tout C. A., 1995, MNRAS, 277, 1443
Hernquist L., 1990, ApJ, 356, 359
Herwig F., 2005, ARA&A, 43, 435
Ho A. Y. Q. et al., 2017, ApJ, 836, 5
Jorissen A., Boffin H. M. J., 1992, in Duquennoy A., Mayor M., eds, Evidences for Interaction among Wide Binary Systems: To Ba or not to Ba? Binaries as Tracers of Stellar Formation. Cambridge Univ. Press, Cambridge, p. 185
Jorissen A., Frayer D. T., Johnson H. W., Mayor M., Smith V. V., 1993, A&A, 271, 463
Jorissen A., Boffin H. M. J., Karinkuzhi D., Van Eck S., Escorza A., Shetye S., Van Winckel H., 2019, A&A, 626, A127
Karakas A. I., Lattanzio C. J., 2003, PASA, 20, 279
Karakas A. I., Lattanzio C. J., 2014, PASA, 31, 30
Karakas A. I., Lugaro M., 2016, ApJS, 825, 26
Karakas A. I., Tout C. A., Lattanzio J. C., 2000, MNRAS, 316, 689
Karakas A. I., Lattanzio C. J., Pols O. R., 2002, PASA, 515, 19
Karakas A. I., Lugaro M., Carlos M., Cseh B., Kamath D., García-Hernández D. A., 2018, MNRAS, 447, 421
Karinkuzhi D. et al., 2018, A&A, 618, A32
Katz D. et al., 2018, A&A, 616, A11
Kelson D. D., Illingworth G. D., van Dokkum P. G., Franx M., 2000, ApJ, 531, 159
Kupka F., Piskunov N., Ryabchikova T. A., Stempels H. C., Weiss W. W., 1999, A&AS, 138, 119
Lindegren L. et al., 2018, A&A, 616, A2
Liu J. H., Zhang B., Liang Y. C., Peng Q. H., 2000, A&A, 363, 660
Luck R. E., Heiter U., 2007, AJ, 133, 2464
Lugaro M., Karakas A. I., Stancliffe R. J., Rijs C., 2012, ApJ, 747, 2
MacConnell D. J., Frye R. L., Upgren A. R., 1972, AJ, 77, 384
McClure R. D., 1983, ApJ, 268, 264
Maiorca E., Randich S., Busso M., Magrini L., Palmerini S., 2011, ApJ, 736, 120
Malaney R. A., Lambert D. L., 1988, MNRAS, 235, 695
Mishenina T. V., Bienaymé O., Gorbaneva T. I., Charbonnel C., 2006, A&A, 456, 1109
Miyamoto M., Nagai R., 1975, PASJ, 27, 533
Mowlavi N., 1999, A&A, 350, 73
Navarro J. F., Frenk C. S., White S. D. M., 1997, ApJ, 490, 493
Ness M., Hogg D. W., Rix H.-W., Ho A. Y. Q., Zasowski G., 2015, ApJ, 808, 16
Ness M., Hogg D. W., Rix H. W., Martig M., Pinsonneault M. H., Ho A., 2016, ApJ, 823, 114
Pereira C. B., Sales Silva J. A., Chavero C., Roig F., Jilinski E., 2011, A&A, 533, A51
Price-Whelan A. M., 2017, Journal of Open Source Software, 2, 388
Price-Whelan A. M., Hogg D. W., Johnston K. V., Hendel D., 2014, ApJ, 4, 794
Prusti T.(Gaia Collaboration) et al. (Gaia Collaboration), 2016, A&A, 595, A1
Sartoretti P. et al., 2018, A&A, 616, A6
Schlafly E. F., Finkbeiner D. P., 2011, ApJ, 737, 103
Shectman S. A., Johns M., 2003, Proc. SPIE, 4837, 910
Slemer A. et al., 2017, MNRAS, 465, 4817
Sneden C., Cowan J. J., Gallino R., 2008, ARA&A, 46, 241
Straniero O., Cristallo S., Piersanti L., 2014, ApJ, 785, 77
Takeda Y., Sato B. V., Murata D., 2008, AJ, 60, 781
Tian Z. et al., 2018, Res. Astron. Astrophys., 18, 52
Travaglio C., Gallino R., Busso M., Gratton R., 2001, ApJ, 549, 346
Valenti J. A., Piskunov N., 1996, A&AS, 118, 595
Van Eck S., Jorissen A., 1999, A&A, 345, 127
Ventura P., Di Criscienzo M., Carini R., D'Antona F., 2013, MNRAS, 431, 3642
Wang H-F., Liu C., Xu Y., Wan J-C., Deng L., 2018, MNRAS, 478, 3367
Webbink R. F., 1986, in Leung K. C., Zhai D. S., eds, Critical Observations versus Physical Models for Close Binary Systems. Gordon and Breach, New York, p. 403
Whitelock P. A., Menzies J. W., Feast M. W., Nsengiyumva F., Matsunaga N., 2013, MNRAS, 428, 2216
Wu Y et al., 2011a, Res. Astron. Astrophys., 11, 924
Wu Y., Singh H. P., Prugniel P., Gupta R., Koleva M., 2011b, A&A, 525, A71

SUPPORTING INFORMATION

Supplementary data are available at *MNRAS* online.

Table 1. Properties of 895 s-process-rich candidates.

Please note: Oxford University Press is not responsible for the content or functionality of any supporting materials supplied by the authors. Any queries (other than missing material) should be directed to the corresponding author for the article.

This paper has been typeset from a TEX/LATEX file prepared by the author.